Analytical Multi-User MIMO Channel Modeling: Subspace Alignment Matters

Nicolai Czink, Bernd Bandemer, Claude Oestges, Thomas Zemen, Arogyaswami Paulraj

***Abstract*—For a receiver that observes a mixture of desired and interfering multiple-input multiple-output (MIMO) transmissions, not all interference has the same severity: its effect is modulated by the degree of alignment between the eigenspaces of the desired and undesired channel matrices.**

An analytical channel model is proposed to account for this effect. Two metrics of eigenspace compatibility are studied, and a method to generate channels of a given degree of compatibility is derived. The resulting model is parameterized using radio channel measurement data, and an implementation recipe for immediate use of the model is provided.

I. Introduction

With multiple-input multiple-output (MIMO) systems penetrating the mass market, the number of multi-antenna devices increases drastically. As a result, the interference from MIMO devices is constantly growing.

Current deployments of MIMO focus on single-user schemes, where MIMO devices are orthogonally addressed, either by time-division or frequency-division multiplex. Future deployments are expected to support space-division multiplex, thus transmitting to or receiving from multiple MIMO users at the same time. This is feasible when the channels to the different users are sufficiently orthogonal in the signal domain.

A. Motivation

Consider the multi-user MIMO channel depicted in Figure 1, where two transmitters (Tx) communicate with a common receiver (Rx). A broadly used channel model for such an environment is the Kronecker model [1], which describes the MIMO channels by separate transmit and receive correlation matrices. Let us consider the receive correlation matrix. If the two transmitters are in close vicinity of each other, the receive correlation matrix of their respective channels will be very similar.[1] On the other hand, if the transmitters are far apart from each other, their channels will expose *distinguishable receive correlation matrices*. In the extreme case of orthogonal correlation matrices, and hence orthogonal signal subspaces from the two transmitters, information can be sent by both transmitters simultaneously without causing interference to each other. Should the signal subspaces of the correlation matrices overlap (which is commonly the case), the channel no longer supports interference-free transmission. Therefore, the alignment of the eigenmodes of the receive correlation matrices has significant impact on the capacity of the interference-impaired channel.

As a numerical example, we compare two extreme cases: Consider a MIMO system with two transmitting users, each equipped with two transmit antennas, and a single receiver with two antennas. Assume that (i) the MIMO channels from both users lead to the same receive correlation matrix $\mathbf{R}_1 = \mathbf{R}_2 = \mathrm{diag}(0.9, 0.1)$, or (ii) the first MIMO channel is characterized by $\mathbf{R}_1 = \mathrm{diag}(0.9, 0.1)$, while the second MIMO channel has $\mathbf{R}_2 = \mathrm{diag}(0.1, 0.9)$. Note that both correlation matrices have the same power and even the same singular values. Generating channels using the (single-sided) Kronecker model, and evaluating the average sum mutual information under interference (in terms of achievable rate) [2] at an SNR of 20 dB, we obtain 6.2 bit/s/Hz for the first case, but 9.2 bit/s/Hz for the second case. Since the singular values of the correlation matrices are exactly the same in both cases, this simple example shows that the alignment of the subspaces can lead to significant data rate improvements in interference scenarios.

In order to capture these effects, new channel models are needed that include effects of receiver-side channel correlation, and therefore, the potential for alignment between different correlation matrices. Such models would allow to evaluate the severity of the interference beyond simple power considerations. So far, no analytical multi-user MIMO channel models are known to the authors that fulfill this requirement.

B. Related Work

Foundational work on multiple-access (interference) channels was published in [3], [4], where the effect of interference from uncorrelated fading was analyzed. Tse and Hanly discussed optimum rate and power allocations for such channels [5], [6].

The influence of interference on MIMO systems was previously studied as well. Dai et al. investigated the influence of MIMO interference on the bit error ratio (BER) of a specific multiuser MIMO system in [7]. Several receiver structures are

This work was partially supported by the European Commission in the framework of the FP7 Network of Excellence in Wireless COMmunications NEWCOM++ (contract no. 216715) and of the FP7 STREPS BuNGee (contract no. 248267), by the Vienna Science and Technology Fund in the FTW project PUCCO, the Austrian Science Fund (FWF) in the project NFN-SISE S10607, and the European COST 2100 Action. The FTW Forschungszentrum Telekommunikation Wien is supported by the Austrian Government and the City of Vienna within the competence center program COMET. The work of C. Oestges is supported by the Belgian Fonds de la Recherche Scientifique (FRS-FNRS). The work of N. Czink was partially supported by an Erwin Schroedinger Fellowship of the Austrian Science Fund (FWF grant number J2789-N14). The work of B. Bandemer is supported by an Eric and Illeana Benhamou Stanford Graduate Fellowship.

[1]Note that "close vicinity" of the tranmitters is slightly oversimplified. What we mean is closeness in the radio propagation sense, which besides geometrical distance includes other effects such as antenna array patterns, the antenna orientation, and shadowing.

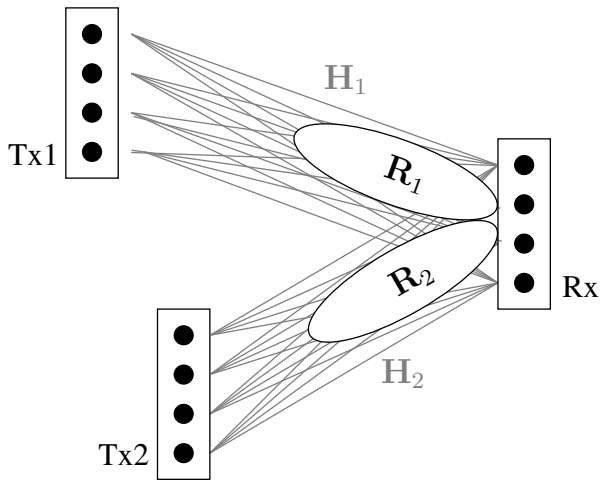

Fig. 1. Multi-user channel from two MIMO Tx to a single MIMO Rx. The individual MIMO channels are denoted by $\mathbf{H}_1, \mathbf{H}_2$. The receive correlation matrices are then given by $\mathbf{R}_i = \mathrm{E}\{\mathbf{H}_i \mathbf{H}_i^{\mathrm{H}}\}$ for $i \in \{1, 2\}$. Note that whenever the two transmitters are not co-located, these receive correlation matrices will differ significantly.

discussed to efficiently combat interference from neighboring cells. However in [7], the interfering channel matrices were assumed to be spatially white, which is a strong simplification. Jiang et al. [8] used an experimental MIMO system and quantified its throughput under interference, and found that the throughput increases when the interference is correlated. Almost concurrently, Blum published a survey article on MIMO transmission under interference, which includes mutual information expressions [2].

Several publications have discussed *signal-processing algorithms* that consider colored noise. Liu et al. [9] have presented an optimum training signal design for correlated MIMO channels under colored interference. However, the simplifying assumption is made that all transmitted signals, regardless of their origin, result in the same receive correlation. The suppression of (strongly correlated) directional interference is discussed in [10]. The authors model the interference as a rank-one signal from a single direction, but this assumption is not supported by real-world measurements. Recently, Rahman et al. [11] discussed the impact of different kinds of interfering signals. It was shown that interference from a space-time coded signal is worst (but can be mitigated with appropriate algorithms). However, the authors used the rich-scattering assumption for both the desired and the interfering signal, which is equivalent to spatially white interference.

Very few previous studies have attempted to *model* correlated interference. A ray-tracing approach is presented in [12], where the authors accurately model an urban scenario with multiple base stations and mobile stations. This modeling approach appears very promising, but the results have not been validated against measurements.

Poutanen et al. [13] introduced a promising geometry-based stochastic approach of "common scatterers", which was adopted by the European COST 2100 model. This idea extends previous cluster-based channel models to include some clusters that are visible only to specific users, while others are visible to all users, which induces correlation between the channels at different users. The authors also exemplify a possible parametrization from a limited set of measurements.

However, to the best of the authors' knowledge, no analytical multi-user MIMO channel models are available that directly model the effect of the relative orientation of the channel eigenspaces (their *alignment*).

C. Contributions

Building on our concepts in [14], we approach the problem of modeling multi-user MIMO channels via their receiver correlation matrices, which provide two spatial signatures: one for the desired signal, the other for the interference. Our main contribution is a method to *vary the relative orientation of the eigenspaces of multi-user channels in a continuous way*.

- We first introduce a class of metrics that reflect the severity of MIMO interference. This class includes interference-impaired mutual information [2], and the Correlation Matrix Distance (CMD) [15]. Such metrics can be expressed in terms of the singular values of the receiver correlation matrices and their corresponding eigenspaces. We show that, given the singular values, these two metrics possess a specific maximum and minimum, which is achieved in certain extreme cases of correlation matrix eigenspace alignment.
- Building on the metrics, we present an analytical multi-user MIMO channel model that generates channel realizations according to a user-chosen level of interference severity. This is achieved by smoothly rotating the eigenspace of the interference correlation matrix.
- Finally, we parameterize our model from multi-user MIMO channel measurements in two different environments and provide a model implementation recipe.

Notation: The superscript $(\cdot)^{\mathrm{H}}$ stands for conjugate (Hermitian) transposition. $\mathrm{E}\{\cdot\}$ denotes the expectation operator, $\mathrm{tr}\{\cdot\}$ the matrix trace, and $\|\cdot\|_{\mathrm{F}}$ the Frobenius norm. $\mathbf{I}$ is the identity matrix of appropriate size. For a matrix $\mathbf{X} = [\mathbf{x}_1, \ldots, \mathbf{x}_N]$, we define the notation $\overleftarrow{\mathbf{X}} = [\mathbf{x}_N, \ldots, \mathbf{x}_1]$, which reverses the order of the columns. We use the word "metric" in the general sense of a scalar function that quantifies an aspect of interest, not in the mathematically rigorous sense of metric spaces.

Organization of the paper: The relevant class of multi-user MIMO metrics is defined in Sections II and III. These metrics are used in Section IV as a basis for the multi-user MIMO channel model. In Section V, the parameterization of the model from measurements is presented. We provide a complete implementation recipe in Section VI. Finally, we draw conclusions in Section VII.

II. Scaled Mutual Information Metric

We first need to quantify the impact of different subspace alignment in order to be able to model it accordingly. To this end, we model an interference-impaired MIMO link by

$$\mathbf{y} = \mathbf{H}_0 \mathbf{x}_0 + \sum_{i=1}^{N} \mathbf{H}_i \mathbf{x}_i + \mathbf{n}, \tag{1}$$

where $\mathbf{H}_0$ denotes the channel matrix carrying the intended signal, $\mathbf{H}_i$ denotes the N interfering channels, $i \in \{1, \ldots, N\}$, and $\mathbf{n} \sim \mathcal{CN}(0, \sigma^2\mathbf{I})$ is complex symmetric white Gaussian noise. We assume that the transmitted symbols are uncorrelated and have unit variance, i.e., $\mathrm{E}\{\mathbf{x}_i\mathbf{x}_i^{\mathrm{H}}\} = \mathbf{I}$, for $i \in \{0, \ldots, N\}$. The channel matrices are of dimensions $D \times T_i$, i.e., the number of transmit antennas can vary between the different links.

We define the $D \times D$ channel correlation matrices at the receiver as

$$\mathbf{R}_0 = \mathrm{E}\left\{\mathbf{H}_0\mathbf{H}_0^{\mathrm{H}}\right\}, \tag{2}$$

$$\mathbf{R}_{\mathrm{I}} = \mathrm{E}\left\{\sum_{i=1}^{N}\mathbf{H}_i\mathbf{H}_i^{\mathrm{H}}\right\}. \tag{3}$$

Furthermore, we write the eigenvalue decompositions of $\mathbf{R}_0$ and $\mathbf{R}_{\mathrm{I}}$ as

$$\mathbf{R}_0 = \mathbf{U}\mathbf{\Lambda}\mathbf{U}^{\mathrm{H}}, \tag{4}$$

$$\mathbf{R}_{\mathrm{I}} = \mathbf{V}\mathbf{\Gamma}\mathbf{V}^{\mathrm{H}}, \tag{5}$$

where $\mathbf{U}$ and $\mathbf{V}$ are unitary matrices, and $\mathbf{\Lambda} = \mathrm{diag}(\lambda_1, \ldots, \lambda_D)$, $\mathbf{\Gamma} = \mathrm{diag}(\gamma_1, \ldots, \gamma_D)$ with sorted eigenvalues $\lambda_1 \geq \lambda_2 \geq \cdots \geq 0$ and $\gamma_1 \geq \gamma_2 \geq \cdots \geq 0$.

In the following, we define the scaled mutual information metric that allows to assess the impact of varying subspace alignment.

A. Metric Definition

Assuming Gaussian signaling at all transmitters, perfect channel state information at the receivers, and single-user detection (treating the interference as noise), the relevant expected mutual information between input $\mathbf{x}_0$ and the output $\mathbf{y}$ of the interference-impaired channel in (1) is given by [2]

$$I = \mathrm{E}\left\{\log_2\det\left(\mathbf{I} + \mathbf{H}_0\mathbf{H}_0^{\mathrm{H}}(\textstyle\sum_i \mathbf{H}_i\mathbf{H}_i^{\mathrm{H}} + \sigma^2\mathbf{I})^{-1}\right)\right\}. \tag{6}$$

Motivated by this equation, we use the correlation matrices $\mathbf{R}_0$ and $\mathbf{R}_{\mathrm{I}}$ instead of the channel matrices and define the mutual information metric

$$\begin{aligned} &J(\mathbf{R}_0, \mathbf{R}_{\mathrm{I}}, \sigma^2) \\ &= \log_2\det\left(\mathbf{I} + \mathbf{R}_0(\mathbf{R}_{\mathrm{I}} + \sigma^2\mathbf{I})^{-1}\right) \\ &= \log_2\det\left(\mathbf{I} + \mathbf{\Lambda}\mathbf{U}^{\mathrm{H}}\mathbf{V}(\sigma^2\mathbf{I} + \mathbf{\Gamma})^{-1}\mathbf{V}^{\mathrm{H}}\mathbf{U}\right) \\ &= \log_2\det\left(\mathbf{I} + \mathbf{\Lambda}\mathbf{Q}(\sigma^2\mathbf{I} + \mathbf{\Gamma})^{-1}\mathbf{Q}^{\mathrm{H}}\right), \end{aligned} \tag{7}$$

where $\mathbf{Q} = \mathbf{U}^{\mathrm{H}}\mathbf{V}$ is a unitary coordinate transformation. For brevity, we occasionally omit the explicit dependence on parameter σ^2 and simply write $J(\mathbf{R}_0, \mathbf{R}_{\mathrm{I}})$.

The value of $J(\mathbf{R}_0, \mathbf{R}_{\mathrm{I}})$ depends on the degree of alignment between the subspaces characterized by $\mathbf{U}$ and $\mathbf{V}$. This is quantified by the following theorem.

Theorem 1. For every $\mathbf{R}_0 = \mathbf{U}\mathbf{\Lambda}\mathbf{U}^{\mathrm{H}}$ and $\mathbf{R}_{\mathrm{I}} = \mathbf{V}\mathbf{\Gamma}\mathbf{V}^{\mathrm{H}}$,

$$\underbrace{J(\mathbf{R}_0, \mathbf{U}\mathbf{\Gamma}\mathbf{U}^{\mathrm{H}})}_{J_{\min}(\mathbf{R}_0, \mathbf{\Gamma})} \leq J(\mathbf{R}_0, \mathbf{V}\mathbf{\Gamma}\mathbf{V}^{\mathrm{H}}) \leq \underbrace{J(\mathbf{R}_0, \overleftarrow{\mathbf{U}}\mathbf{\Gamma}\overleftarrow{\mathbf{U}}^{\mathrm{H}})}_{J_{\max}(\mathbf{R}_0, \mathbf{\Gamma})}. \tag{8}$$

Proof: See Appendix A. ∎

In other words, if we fix $\mathbf{R}_0$ and an eigenvalue profile $\mathbf{\Gamma}$, and then vary $\mathbf{V}$, the two extreme values of $J(\mathbf{R}_0, \mathbf{R}_{\mathrm{I}} = \mathbf{V}\mathbf{\Gamma}\mathbf{V}^{\mathrm{H}})$ are realized by $\mathbf{V} = \mathbf{U}$ (i.e., $\mathbf{Q} = \mathbf{I}$) and $\mathbf{V} = \overleftarrow{\mathbf{U}}$ (i.e., $\mathbf{Q} = \overleftarrow{\mathbf{I}}$). Recall that $\overleftarrow{\mathbf{U}}$ denotes the reversed order of columns of matrix $\mathbf{U}$. Intuitively, the worst case interference occurs when the eigenspaces of signal and interference are identical and thus, the strongest interference mode affects the strongest signal mode. Conversely, the best case (corresponding to the largest mutual information metric) occurs when the strongest eigenmode of the interference aligns with the weakest eigenmode of the signal and vice versa.[2]

The minimum and maximum value are explicitly given by

$$J_{\min}(\mathbf{R}_0, \mathbf{\Gamma}) = \sum_{d=1}^{D}\log_2\left(1 + \lambda_d(\sigma^2 + \gamma_d)^{-1}\right) \tag{9}$$

$$J_{\max}(\mathbf{R}_0, \mathbf{\Gamma}) = \sum_{d=1}^{D}\log_2\left(1 + \lambda_{D+1-d}(\sigma^2 + \gamma_d)^{-1}\right) \tag{10}$$

To emphasize the role of the subspace alignment, we define the scaled metric

$$\tilde{J}(\mathbf{R}_0, \mathbf{R}_{\mathrm{I}}) = \frac{J(\mathbf{R}_0, \mathbf{R}_{\mathrm{I}}) - J_{\min}(\mathbf{R}_0, \mathbf{\Gamma})}{J_{\max}(\mathbf{R}_0, \mathbf{\Gamma}) - J_{\min}(\mathbf{R}_0, \mathbf{\Gamma})}, \tag{11}$$

where $\mathbf{\Gamma}$ is the eigenvalue profile of $\mathbf{R}_{\mathrm{I}}$. This quantity is well-defined unless $J_{\min} = J_{\max}$, which happens when $\mathbf{R}_0$ or $\mathbf{R}_{\mathrm{I}}$ is a multiple of the identity matrix — a degenerate case that we exclude here. Theorem 1 ensures

$$0 \leq \tilde{J}(\mathbf{R}_0, \mathbf{R}_{\mathrm{I}}) \leq 1. \tag{12}$$

In addition, this definition has the following useful property:

Theorem 2. The scaled mutual information metric $\tilde{J}$ is symmetric in its arguments $\mathbf{R}_0$ and $\mathbf{R}_{\mathrm{I}}$, i.e.,

$$\tilde{J}(\mathbf{R}_0, \mathbf{R}_{\mathrm{I}}) = \tilde{J}(\mathbf{R}_{\mathrm{I}}, \mathbf{R}_0). \tag{13}$$

This property permits us to think of $\tilde{J}$ as a measure of compatibility between $\mathbf{R}_0$ and $\mathbf{R}_{\mathrm{I}}$.

Proof: See Appendix B. ∎

B. Evaluation of the Scaled Mutual Information Metric $\tilde{J}$

In this section, we evaluate the quality of the approximation $\tilde{J}$ in (11) with respect to the expected mutual information I in (6). Since $\tilde{J}$ is scaled to the interval $[0, 1]$, we first define a comparably scaled version of I as follows. For simplicity, consider the case with a single interferer, $N = 1$. We model the square channel matrices $\mathbf{H}_0$ and $\mathbf{H}_1$ as complex Gaussian with receiver-side correlation, i.e.,

$$\mathbf{H}_0 = \mathbf{R}_0^{1/2}\mathbf{G}_0, \tag{14}$$

$$\mathbf{H}_1 = \mathbf{R}_{\mathrm{I}}^{1/2}\mathbf{G}_1, \tag{15}$$

where $\mathbf{G}_0$ and $\mathbf{G}_1$ are $D \times D$ matrices with independent entries drawn from $\mathcal{CN}(0, 1)$, and $\mathbf{R}_0$ and $\mathbf{R}_{\mathrm{I}}$ are fixed. Under this model, the expected mutual information I of (6) becomes a function $I(\mathbf{R}_0, \mathbf{R}_{\mathrm{I}})$ of the correlation matrices $\mathbf{R}_0$ and

[2] If $\mathbf{\Lambda}$ and $\mathbf{\Gamma}$ have repeated eigenvalues, there may be more than one matrix $\mathbf{V}$ that achieves the best and worst case metric value, respectively.

$\mathbf{R}_{\mathrm{I}}$. Recalling the eigenvalue decompositions $\mathbf{R}_0 = \mathbf{U}\mathbf{\Lambda}\mathbf{U}^{\mathrm{H}}$ and $\mathbf{R}_{\mathrm{I}} = \mathbf{V}\mathbf{\Gamma}\mathbf{V}^{\mathrm{H}}$, we define the scaled expected mutual information analogously to (11) as

$$\tilde{I}(\mathbf{R}_0, \mathbf{R}_{\mathrm{I}}) = \frac{I(\mathbf{R}_0, \mathbf{R}_{\mathrm{I}}) - I(\mathbf{R}_0, \mathbf{U}\mathbf{\Gamma}\mathbf{U}^{\mathrm{H}})}{I(\mathbf{R}_0, \overleftarrow{\mathbf{U}}\mathbf{\Gamma}\overleftarrow{\mathbf{U}}^{\mathrm{H}}) - I(\mathbf{R}_0, \mathbf{U}\mathbf{\Gamma}\mathbf{U}^{\mathrm{H}})}. \tag{16}$$

Figure 2(a) is a scatter plot of $\tilde{I}(\mathbf{R}_0, \mathbf{R}_{\mathrm{I}})$ versus $\tilde{J}(\mathbf{R}_0, \mathbf{R}_{\mathrm{I}})$ for the case with $D = 4$ antennas. Each of the 50 points in the plot corresponds to a particular choice of $\mathbf{R}_0$ and $\mathbf{R}_{\mathrm{I}}$. The $\tilde{J}$ coordinate is computed directly from (11), while the expected values in the $\tilde{I}$ expression (16) are numerically evaluated using 10^5 Monte-Carlo channel realizations. For each point in the plot, $\mathbf{R}_0$ and $\mathbf{R}_{\mathrm{I}}$ were drawn independently of each other based on the eigenvalue decompositions $\mathbf{U}\mathbf{\Lambda}\mathbf{U}^{\mathrm{H}}$ and $\mathbf{V}\mathbf{\Gamma}\mathbf{V}^{\mathrm{H}}$. The matrices $\mathbf{U}$ and $\mathbf{V}$ were drawn uniformly over the set of unitary matrices. The diagonal elements of $\mathbf{\Lambda}$ and $\mathbf{\Gamma}$ were drawn independently from exponential distributions with mean $100\sigma^2$ and $10\sigma^2$, respectively, corresponding to a signal-to-noise ratio of 20 dB and interference-to-noise ratio 10 dB.

We conclude that the scaled approximation $\tilde{J}$ captures the behavior of the scaled mean mutual information $\tilde{I}$ very well. In fact, in some special cases, the two empirically coincide. This occurs when (a) $\mathbf{R}_0$ is chosen according to the single-parameter model (27), and (b) the eigenvalues of $\mathbf{R}_{\mathrm{I}}$ coincide with those of $\mathbf{R}_0$, i.e., $\mathbf{\Gamma} = \mathbf{\Lambda}$. An example for this case is shown in Figure 2(b), where we have set $\mu = 0.9$ and $D = 4$ in (27), and SNR and INR are 20 dB. Since $\mathbf{R}_0$ and $\mathbf{\Gamma}$ are fixed, each point in the scatter plot corresponds to a particular choice of $\mathbf{V}$. As before, the expression for $\tilde{I}$ (16) is computed using 10^5 Monte-Carlo channels.

In summary, $\tilde{J}$ models the behaviour of the true expected mutual information I in (6) very well under appropriate linear scaling. Therefore, the metric $\tilde{J}$ is very practical since it directly describes the ultimate performance limits given a certain interference. Note that this approach can be extended to include transmit precoding by including the corresponding precoding matrix into the mutual information equation as demonstrated in [2].

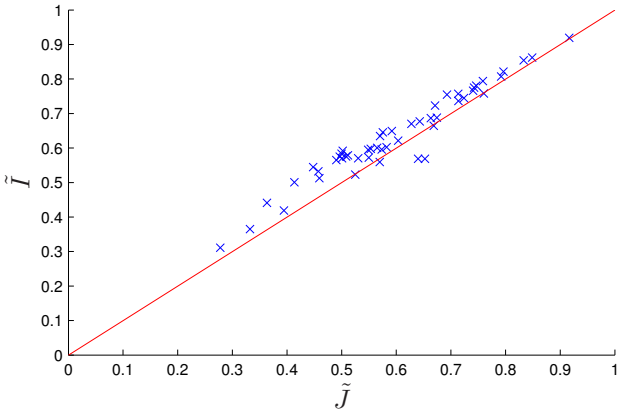

(a) $\mathbf{R}_0$ and $\mathbf{R}_{\mathrm{I}}$ independent with exponential eigenvalues

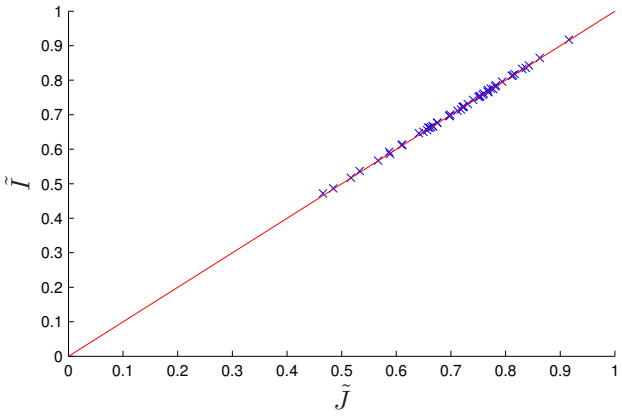

(b) $\mathbf{R}_0$ fixed according to (27) and $\mathbf{R}_{\mathrm{I}}$ such that $\mathbf{\Gamma} = \mathbf{\Lambda}$

Fig. 2. Scatter plots of the scaled approximate mutual information metric $\tilde{J}$ used in our model and the scaled expected mutual information $\tilde{I}$, for 50 choices of $\mathbf{R}_0$ and $\mathbf{R}_{\mathrm{I}}$.

III. Other Metrics

The metric $\tilde{J}$ as defined in Section II-A is a specific way to model channel interaction in interference-impaired MIMO communication. Apart from this particular choice, the model proposed in the next section works with any alternative metric that fulfills the following requirements:

- The metric depends on $\mathbf{R}_0 = \mathbf{U}\mathbf{\Lambda}\mathbf{U}^{\mathrm{H}}$ and $\mathbf{R}_{\mathrm{I}} = \mathbf{V}\mathbf{\Gamma}\mathbf{V}^{\mathrm{H}}$.
- For fixed $\mathbf{R}_0 = \mathbf{U}\mathbf{\Lambda}\mathbf{U}^{\mathrm{H}}$ and $\mathbf{\Gamma}$, it reaches its extreme values for $\mathbf{V} = \mathbf{U}$ and $\mathbf{V} = \overleftarrow{\mathbf{U}}$.
- The metric is continuous in $\mathbf{V}$.

An example for an alternative metric is the correlation matrix distance (CMD) as given below.

A. Correlation Matrix Distance

The CMD was introduced by Herdin et al. [15] in order to quantify the distance between measured channel correlation matrices. The CMD is defined as

$$d(\mathbf{R}_0, \mathbf{R}_{\mathrm{I}}) = 1 - \frac{\mathrm{tr}\{\mathbf{R}_0\mathbf{R}_{\mathrm{I}}\}}{\|\mathbf{R}_0\|_{\mathrm{F}} \cdot \|\mathbf{R}_{\mathrm{I}}\|_{\mathrm{F}}}. \tag{17}$$

By definition, this metric is symmetric in its arguments $\mathbf{R}_0$ and $\mathbf{R}_{\mathrm{I}}$ and is bounded between 0 ($\mathbf{R}_0$ and $\mathbf{R}_{\mathrm{I}}$ are collinear) and 1 (the matrices do not share any common subspace). Using the eigenvalue decompositions and $\mathbf{Q} = \mathbf{U}^{\mathrm{H}}\mathbf{V}$, it can be rewritten as

$$d(\mathbf{R}_0, \mathbf{R}_{\mathrm{I}}) = 1 - \frac{\mathrm{tr}(\mathbf{\Lambda}\mathbf{Q}\mathbf{\Gamma}\mathbf{Q}^{\mathrm{H}})}{\sqrt{\mathrm{tr}(\mathbf{\Lambda}^2)\mathrm{tr}(\mathbf{\Gamma}^2)}}. \tag{18}$$

Tight bounds on the metric are given as follows.

Theorem 3. For fixed $\mathbf{R}_0 = \mathbf{U}\mathbf{\Lambda}\mathbf{U}^{\mathrm{H}}$ and $\mathbf{\Gamma}$,

$$\underbrace{d(\mathbf{R}_0, \mathbf{U}\mathbf{\Gamma}\mathbf{U}^{\mathrm{H}})}_{d_{\min}} \leq d(\mathbf{R}_0, \mathbf{V}\mathbf{\Gamma}\mathbf{V}^{\mathrm{H}}) \leq \underbrace{d(\mathbf{R}_0, \overleftarrow{\mathbf{U}}\mathbf{\Gamma}\overleftarrow{\mathbf{U}}^{\mathrm{H}})}_{d_{\max}}, \tag{19}$$

for all unitary matrices $\mathbf{V}$.

Proof: See Appendix C. ∎

As in Section II-A, the two extreme cases are realized by $\mathbf{V} = \mathbf{U}$ (i.e., $\mathbf{Q} = \mathbf{I}$) and $\mathbf{V} = \overleftarrow{\mathbf{U}}$ (i.e., $\mathbf{Q} = \overleftarrow{\mathbf{I}}$). The minimum and maximum value can be explicitly evaluated as

$$d_{\min} = 1 - \frac{\sum_{d=1}^{D} \lambda_d \gamma_d}{\sqrt{\left(\sum_{d=1}^{D} \lambda_d^2\right)\left(\sum_{d=1}^{D} \gamma_d^2\right)}}, \tag{20}$$

$$d_{\max} = 1 - \frac{\sum_{d=1}^{D} \lambda_{D+1-d} \cdot \gamma_d}{\sqrt{\left(\sum_{d=1}^{D} \lambda_d^2\right)\left(\sum_{d=1}^{D} \gamma_d^2\right)}}. \tag{21}$$

The structure of this metric is similar to the mutual information metric. The advantage of the CMD as metric is that it compares the *normalized* channels (cf. the denominator in (17)) and is therefore more sensitive to differences in the correlation structure. Unfortunately, no direct interpretation in terms of communication performance based on the CMD has been derived yet.

IV. Modeling the Multi-user Channel Subspaces

In this section, instead of computing channel alignment metrics for given channel conditions, we consider the inverse problem of generating channels for given values of the metrics.

A. General Modeling Principle

Upper and lower bounds on system performance under several metrics, such as the ones defined in the previous section, are determined by the eigenvalue structure of the receiver correlation matrices. The actual performance, however, is strongly affected by the relative alignment of their eigenspaces as captured by the coordinate transform $\mathbf{Q}$. In order to test MU-MIMO algorithms for their performance, they need to be evaluated under varying channels conditions that cover the entire spectrum of possible signal subspace alignments.

The procedure presented in this section generates receiver correlation matrices for this purpose. Recall that the received spatial signatures are $\mathbf{R}_0 = \mathbf{U}\mathbf{\Lambda}\mathbf{U}^{\mathrm{H}}$ and $\mathbf{R}_{\mathrm{I}} = \mathbf{V}\mathbf{\Gamma}\mathbf{V}^{\mathrm{H}}$. We assume that the spatial signature $\mathbf{R}_0$ of the desired signal, the eigenvalue profile $\mathbf{\Gamma}$ of the interference, and the noise power σ^2, are pre-specified. They may be obtained from measurements or from a qualified link model (we outline an implementation recipe in Section VI).

In addition, a target point for the alignment of the subspaces needs to be specified. The alignment is quantified by one of the previously discussed metrics, within the bounds of (12) and (19). Our model generates a suitable $\mathbf{V}$ such that the metric meets the target, i.e., the pre-specified $\mathbf{R}_0$ and the generated $\mathbf{R}_{\mathrm{I}}$ are related as desired.

In the following, we describe the procedure in detail for the mutual information metric $\tilde{J}$, but it applies likewise for any metric that satisfies the requirements of Section III. The procedure can in principle also be used to generate channel matrices instead of correlation matrices.

B. Generation of a Deterministic $\mathbf{V}$

We are given $\mathbf{R}_0 = \mathbf{U}\mathbf{\Lambda}\mathbf{U}^{\mathrm{H}}$, $\mathbf{\Gamma}$, and $\tilde{J}_{\text{target}}$. Our task is to find a $\mathbf{V}$ that satisfies $\tilde{J}(\mathbf{R}_0, \mathbf{V}\mathbf{\Gamma}\mathbf{V}^{\mathrm{H}}) = \tilde{J}_{\text{target}}$.

A solution exists only if $0 \le \tilde{J}_{\text{target}} \le 1$. Theorem 1 shows that $\tilde{J} = 0$ is achieved by $\mathbf{V} = \mathbf{U}$, while $\tilde{J} = 1$ is attained by $\mathbf{V} = \overleftarrow{\mathbf{U}}$. Therefore, a $\mathbf{V}$ that meets $\tilde{J}_{\text{target}}$ must exist along a smooth unitary curve from $\mathbf{U}$ to $\overleftarrow{\mathbf{U}}$. Such a curve can be defined rigorously as follows.

Definition 1. Let $\mathbf{Z}$ be a unitary matrix. Define

$$P_{\mathbf{I}\to\mathbf{Z}}(s) = \mathbf{W}\mathrm{e}^{js\mathbf{\Phi}}\mathbf{W}^{\mathrm{H}}, \qquad \text{for } s \in [0,1], \tag{22}$$

where $\mathbf{W}$ and $\mathbf{\Phi}$ follow from the eigenvalue decomposition $\mathbf{Z} = \mathbf{W}\mathrm{e}^{j\mathbf{\Phi}}\mathbf{W}^{\mathrm{H}}$, in which $\mathbf{\Phi} = \operatorname{diag}(\phi_1, \ldots, \phi_n)$ is a diagonal matrix of phase angles in $(-\pi, \pi]$, and the matrix exponential is given as $\mathrm{e}^{js\mathbf{\Phi}} = \operatorname{diag}(\mathrm{e}^{js\phi_1}, \ldots, \mathrm{e}^{js\phi_n})$.

Definition 2. Let $\mathbf{Z}_1$, $\mathbf{Z}_2$ be unitary matrices. Define

$$P_{\mathbf{Z}_1\to\mathbf{Z}_2}(s) = \mathbf{Z}_1 \cdot P_{\mathbf{I}\to\mathbf{Z}_1^{-1}\mathbf{Z}_2}(s), \qquad \text{for } s \in [0,1]. \tag{23}$$

It is clear that the end points of this curve are $P_{\mathbf{Z}_1\to\mathbf{Z}_2}(0) = \mathbf{Z}_1$ and $P_{\mathbf{Z}_1\to\mathbf{Z}_2}(1) = \mathbf{Z}_2$. Furthermore, $P_{\mathbf{Z}_1\to\mathbf{Z}_2}(s)$ is unitary for all $s \in [0,1]$.

For our specific case, the subspace model is given by

$$\mathbf{V}(s) = P_{\mathbf{U}\to\overleftarrow{\mathbf{U}}}(s), \tag{24}$$

and $\tilde{J}(s) = \tilde{J}(\mathbf{R}_0, \mathbf{V}(s)\mathbf{\Gamma}\mathbf{V}(s)^{\mathrm{H}})$. Note that $\tilde{J}(s)$ is a continuous function. (It is not necessarily monotonic.) Since $\tilde{J}(0) = 0$, and $\tilde{J}(1) = 1$, we are guaranteed the existence of an $s^\star \in [0,1]$ with $\tilde{J}(s^\star) = \tilde{J}_{\text{target}}$. This $s^\star$ can be calculated to arbitrary precision by the bisection method [16]. The desired subspace matrix is then $\mathbf{V}(s^\star)$.

C. Generation of a Random $\mathbf{V}$

The previous approach generates a deterministic $\mathbf{V}$ that achieves the desired $\tilde{J}_{\text{target}}$. However, in general, there exist infinitely many possible solutions for $\mathbf{V}$. Different values of $\mathbf{V}$, even though leading to the same mutual information metric, may lead to different system performance. To test the impact on the system, the interference model must be able to sample the entire solution space. To this end, we provide the following algorithm.

1) Draw a unitary matrix $\mathbf{Z}$ uniformly at random.
2) Evaluate $\tilde{J}_{\mathbf{Z}} = \tilde{J}(\mathbf{R}_0, \mathbf{Z}\mathbf{\Gamma}\mathbf{Z}^{\mathrm{H}})$.
3) Consider the curve

$$\mathbf{V}(s) = \begin{cases} P_{\mathbf{U}\to\mathbf{Z}}(s) & \text{if } \tilde{J}_{\text{target}} \le \tilde{J}_{\mathbf{Z}} \\ P_{\mathbf{Z}\to\overleftarrow{\mathbf{U}}}(s) & \text{if } \tilde{J}_{\mathbf{Z}} < \tilde{J}_{\text{target}}, \end{cases} \tag{25}$$

and the corresponding mutual information function

$$\tilde{J}(s) = \tilde{J}(\mathbf{R}_0, \mathbf{V}(s)\mathbf{\Gamma}\mathbf{V}(s)^{\mathrm{H}}). \tag{26}$$

4) Find $s^\star \in [0,1]$ such that $\tilde{J}(s^\star) = \tilde{J}_{\text{target}}$ using the bisection method and return $\mathbf{V}(s^\star)$.

Step 1 can be easily implemented by computing the matrix of left singular vectors of a random complex Gaussian matrix. After Step 3, we certainly have $\tilde{J}(0) \le \tilde{J}_{\text{target}} \le \tilde{J}(1)$. Since $\tilde{J}(s)$ is continuous, the bisection method in Step 4 will always succeed.

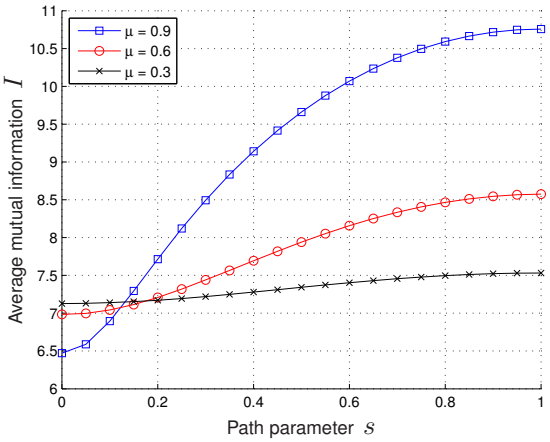

Fig. 3. Average mutual information of multi-user interference channels with different alignments of signal and interference subspace. For $s = 0$, signal and interference subspace are completely overlapping, while for $s = 1$, the strongest interference eigenvector couples into the weakest signal eigenvector.

D. Numerical Example

To demonstrate the effect of subspace alignment on system performance, and to illustrate the path-based methods of Sections IV-B and IV-C, we consider the following example. Assume the simple receiver correlation structure [17]

$$\mathbf{R}_0 = \begin{bmatrix} \mu^0 & \mu^1 & \cdots & \mu^{D-1} \\ \mu^1 & \mu^0 & \ddots & \vdots \\ \vdots & \ddots & \ddots & \vdots \\ \mu^{D-1} & \cdots & \mu^1 & \mu^0 \end{bmatrix} = \mathbf{U}\mathbf{\Lambda}\mathbf{U}^{\mathrm{H}}, \qquad (27)$$

where the inter-antenna correlation μ ranges between 0.3 (rather uncorrelated channels) and 0.9 (highly correlated channels). To model the interference correlation $\mathbf{R}_{\mathrm{I}} = \mathbf{V}^{\mathrm{H}}\mathbf{\Gamma}\mathbf{V}$, we use $\mathbf{\Gamma} = \mathbf{\Lambda}$ for simplicity. We generate $\mathbf{V}(s)$ for $s \in [0, 1]$ as described in Section IV-B. We use $D = 4$ and $\mu \in \{0.3, 0.6, 0.9\}$. Furthermore, we assume the desired and interfering channels to have the same power on average, with signal-to-noise and interference-to-noise ratio of 20 dB.

Figure 3 depicts the expected mutual information I under interference according to (6) as computed by Monte-Carlo averaging of the modeled channels. It is surprising how strongly this quantity changes solely due to the rotations of the interference eigenspace. For low correlations ($\mu = 0.3$) changes of around 10 % of mutual information are seen compared to the minimum value, while for high correlations ($\mu = 0.9$) changes of more than 65 % are possible.

V. Parameterization from Measurements

In this section, we demonstrate by two examples how the multi-user MIMO model can be parameterized from radio channel measurements.

A. Environments

We investigated two kinds of environments: peer-to-peer nomadic channels in an indoor office environment, and micro-cellular mobile channels in an indoor-to-outdoor environment.

Fig. 4. Indoor 2×2 configuration (stars represent transmit arrays, diamonds represent receive arrays): each two-antenna node was located in the indicated room, but symbols do not indicate the exact location within the room

1) Indoor-to-indoor Nomadic Channels: The first experimental parameterization relies on 2×2 nomadic peer-to-peer channels measured in a typical European office environment (in Louvain-la-Neuve, Belgium). The scenario consists of different rooms aligned along a corridor and separated by brick or plasterboard walls [18]. The channel was measured by means of the UCL-ULB Elektrobit channel sounder at 3.8 GHz transmitting at a power of 23 dBm, using a null-to-null bandwidth of 50 MHz, which reduces to 15 MHz arranged in 121 frequency bins after post-processing. The experimental configuration involved 4 transmit and 4 receive antenna arrays, each array consisting of two dipoles separated by half a wavelength. The antenna arrays were located as indicated in Figure 4 with random orientation. There is a total of 16 links $n \rightarrow m$, with transmitter index n and receiver index m, with $m, n \in \{1, 2, 3, 4\}$. For measuring nomadic channels, the location of the arrays was fixed, while there was mobility in the environment, i.e. people, were moving. The minimum peak-to-noise ratio in the power delay profile was found to be 6 dB, however, the measurement SNR was increased by zeroing noise samples in the impulse response.

2) Indoor-to-Outdoor Mobile Channels: The second setup is based on indoor-to-outdoor MIMO channel measurements in a 4×2 configuration, where 2-antenna transmitters were moved indoors along well-defined routes [19], as illustrated in Figure 5. The receiver had 2 dual-polarized patch antennas (resulting in 4 antenna elements) at a height of 10 m and was located outdoors approximately 45 m away, directed towards the office building. The latter is a cubicle-style office environment in Santa Clara, California. The Stanford RUSK channel sounder was operated at a transmit power of 23 dBm at a center frequency of 2.45 GHz with a bandwidth of 70 MHz arranged in 224 frequency bins. The minimum peak-to-noise ratio in the power delay profile was 10 dB.

B. Parameter Estimation

1) Indoor-to-indoor Nomadic Channels: As all channels are static in this scenario, the mutual information metric is calculated based on the receive correlation matrices on each frequency tone over the (effective) measurement bandwidth of 15 MHz (the receive correlation matrix is obtained as given

Fig. 5. Indoor-to-outdoor environment and indoor floor plan. The asterisk denotes the matching corner.

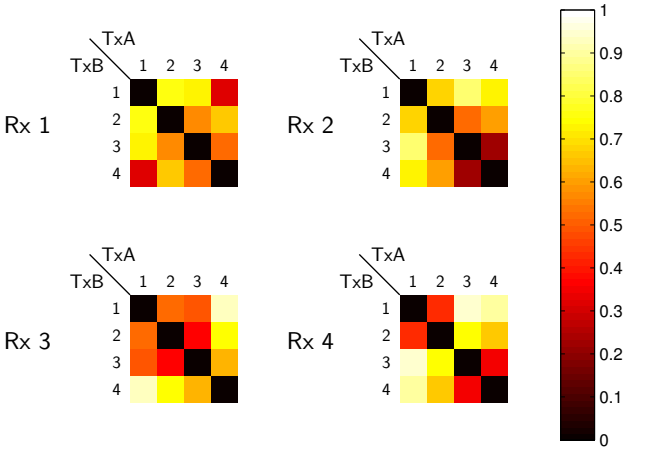

Fig. 6. Scaled mutual information metric $\tilde{J}$ for all link pairs sharing a common receive array

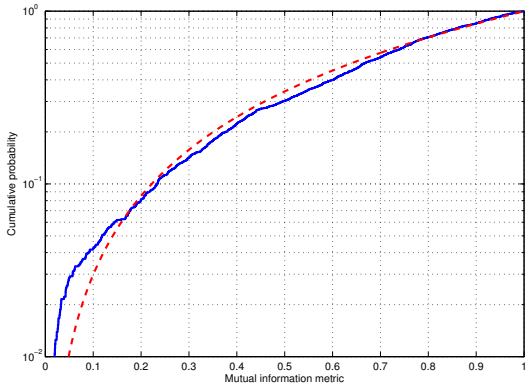

Fig. 7. Empirical (solid line) and fitted Beta (dashed line) distributions of $\tilde{J}$

by (2)-(3), where the expectation is taken over time instants) [18], [20]. We consider all pairs of links with a common receiver, i.e., all combinations of $n_1 \to m$ and $n_2 \to m$, where $n_1, n_2, m \in \{1, \ldots, 4\}$ and $n_1 \neq n_2$, and investigate the metric distribution over the frequency tones, corresponding to possible static channel realizations.

The frequency-averaged metric between such link pairs is depicted in Figure 6. It can be observed that the metric varies significantly from one pair to another: as an example, it is very large between links $1 \to 3$ and $4 \to 3$, whereas it is very close to zero for links $3 \to 2$ and $4 \to 2$. A possible explanation is that for link pairs characterized by a low distance (in terms of $\tilde{J}$), the signals mainly reach the receiver via the room door, irrespective of where they were transmitted from, therefore increasing the similarity between the receive correlation subspaces. For example, it could be argued that the propagation on link $1 \to 3$ is via the corridor and doors, while the main propagation path for $4 \to 3$ passes through the walls. Hence, the links are well-separated, resulting in an increased mutual information metric. Conjecturably, the metric would depend on the balance between the through-wall contribution and the corridor wave-guiding contribution. However, this investigation is beyond the scope of this paper, as the metric is also impacted by the array orientation, as pointed out in Section I-A.

As a model parameter, we use the *distribution of* $\tilde{J}$ over all distinct link pairs, as illustrated in Figure 7. It is well approximated by a Beta distribution,

$$p_\beta(\tilde{J}) = \frac{\Gamma(a+b)}{\Gamma(a)\Gamma(b)} \tilde{J}^{a-1}(1-\tilde{J})^{b-1} \tag{28}$$

where $\Gamma(\cdot)$ is the Gamma function. The Beta distribution (whose match is confirmed by a Kolmogorov-Smirnov goodness-of-fit test at a significance of 5%) is particularly adequate to describe the metric statistics, as it is bounded between 0 and 1, analogous to $\tilde{J}$. From our data, we estimated $a = 1.51$ and $b = 0.98$.

The distributions of the eigenvalues in $\mathbf{\Lambda}$ and $\mathbf{\Gamma}$ are found to be similar for all link pairs, which is a consequence of the peer-to-peer context. Note that this does not contradict the fact that the metric varies between different link pairs. Even though the eigenvalue distributions are similar for all the links, the subspace alignment is not, and therefore it is reasonable that the metric will be different for different links. Furthermore, since the receive correlation is described by 2×2 matrices, the eigenvalue distribution can be characterized by the distribution of their condition number $\kappa = \lambda_0/\lambda_1$. The empirical distribution of κ is found to be well approximated by a lognormal distribution. In other words, κ is Gaussian distributed when expressed in decibels, with a mean of 12.6 dB and a standard deviation of 6.2 dB.

Based on the distribution of $\tilde{J}$ and the eigenvalues, the analytical model can therefore be implemented as described in Section VI.

2) Indoor-to-outdoor Mobile Channels: Receive correlation matrices were estimated from the data using a sliding window over short-term stationary periods. Exact details are provided in [19]. The distribution of the mutual information metric for both investigated pairs of links is depicted in Figure 8, together with their respective Beta distribution fit (again, the Beta fitting

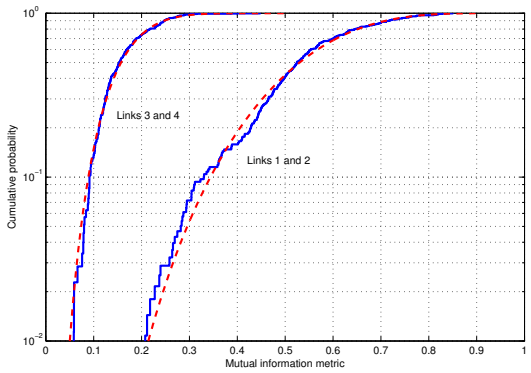

Fig. 8. Empirical (solid line) and fitted Beta (dashed line) distributions of $\tilde{J}$

was confirmed by a Kolmogorov-Smirnov goodness-of-fit test at a significance of 5%):

- between routes 1 and 2, $a = 6.24$, $b = 5.56$,
- between routes 3 and 4, $a = 5.66$, $b = 28.86$.

Interestingly, the distance between links 3 and 4 (in terms of $\tilde{J}$) is significantly smaller than the distance between links 1 and 2. Intuitively, this means that both transmitters (on links 3 and 4) have the same array orientation and communicate towards the outdoor receiver via the same propagation paths, probably through the right-side wall. By contrast, the signals transmitted on routes 1 and 2 reach the outdoor receiver through different propagation paths. Given the environment layout, one may safely assume that the main propagation path on route 1 is through the upper right corner (indicated by the asterisk) directly to the receiver, whereas on route 2, propagation mostly takes place through the right-side wall and then diffraction on a neighboring building towards the receiver. Hence, routes 1 and 2 are well separated, since the corresponding propagation paths do not significantly intersect from the outdoor receiver viewpoint.

We found that the eigenvalue distribution might differ substantially between the links involved (except for links 3 and 4, which have essentially the same marginal statistics). Hence, they are evaluated separately. We found that all eigenvalue distributions could be well approximated by a lognormal distribution. The mean and standard deviation of the best-fit Gaussian distributions are summarized in Table I. It can be observed that the eigenvalue distributions on links 2 and 3/4 are actually quite similar, while being largely different on route 1. This confirms the previous discussion on the differentiated propagation paths, i.e., that the main propagation path for links 2, 3 and 4 is via the right-side wall, unlike link 1.

TABLE I. Eigenvalue distributions in indoor-to-outdoor scenarios

Link index	Sorted eigenvalue index	Mean (dB)	Std (dB)
1	1	4.09	0.68
	2	-0.78	1.53
	3	-4.89	1.84
	4	-8.12	1.60
2	1	3.63	0.40
	2	0.03	0.63
	3	-3.75	0.95
	4	-6.37	0.92
3/4	1	3.18	0.53
	2	0.07	0.71
	3	-2.42	0.99
	4	-5.61	1.16

VI. Implementation Recipe

In this section, we present an implementation recipe to generate multi-user MIMO channel matrices for algorithm testing.

First of all, the metric reflecting the subspace alignment needs to be chosen. For simplicity of notation, we will use the mutual information metric $\tilde{J}$, but the implementation recipe is similar for any other chosen metric. We exemplify the implementation for systems with two antennas, thus describing the singular value profiles by the respective condition numbers κ_0 (for the subspace of the intended signal) and κ_I (for the interference subspaces).

There are two options in terms of how the algorithm under test shall be evaluated: (i) the algorithm shall be tested against realistic values of $\tilde{J}$ in a chosen radio environment; (ii) the algorithm performance shall be thoroughly quantified for all values of $\tilde{J}$, and for varying eigenvalue profiles. Depending on the options, different implementations should be considered.

A. Performance Testing with Realistic Channel Parameters

After parameterization from measurements as shown in Section V, the model can be used for algorithm performance testing yielding realistic results.

Channels are generated using the following method.

1) Define the environment by choosing the parameter distributions $p(\tilde{J}_\mathrm{target})$, $p(\kappa_0)$, and $p(\kappa_\mathrm{I})$.
2) Draw multiple realizations of $(\tilde{J}_\mathrm{target}, \kappa_0, \kappa_\mathrm{I})$, representing different realizations of the chosen environment
3) For each realization of $(\tilde{J}_\mathrm{target}, \kappa_0, \kappa_\mathrm{I})$
   a) Calculate correlation matrices:

$$\mathbf{R}_0 = \frac{2}{1+\kappa_0}\,\mathbf{U}\begin{bmatrix}\kappa_0 & 0\\ 0 & 1\end{bmatrix}\mathbf{U}^\mathrm{H}, \text{ with} \tag{29}$$

$$\mathbf{U} \text{ being a random unitary matrix,} \tag{30}$$

$$\mathbf{\Gamma} = \frac{2}{1+\kappa_\mathrm{I}}\begin{bmatrix}\kappa_\mathrm{I} & 0\\ 0 & 1\end{bmatrix}, \text{ and} \tag{31}$$

$$\mathbf{V}, \text{ such that } \tilde{J}(\mathbf{R}_0, \mathbf{V}\mathbf{\Gamma}\mathbf{V}^\mathrm{H}) = \tilde{J}_\mathrm{target}. \tag{32}$$

   The matrix $\mathbf{V}$ in (32) is obtained as described in Section IV-B or Section IV-C.

   b) Draw multiple realizations of channel matrices:

$$\mathbf{H}_0 = \mathbf{R}_0^{1/2}\mathbf{G}_0, \tag{33}$$

$$\mathbf{H}_I = \mathbf{V}\mathbf{\Gamma}^{1/2}\mathbf{V}^\mathrm{H}\mathbf{G}_\mathrm{I}, \tag{34}$$

   where $\mathbf{G}_0$ and $\mathbf{G}_\mathrm{I}$ contain i.i.d. $\mathcal{CN}(0,1)$ samples.

   c) Test the algorithm using the generated channel matrices.

B. Thorough Performance Analysis

In some environments, like in indoor peer-to-peer networks, we observed that the metric $\tilde{J}$ takes on all possible values. In

this case, it may be reasonable to quantify the performance of the algorithm under test for all possible values of $\tilde{J}$ under varying singular value profiles.

The corresponding method is as follows.

1) Select a grid of values for
   - $\tilde{J}_{\text{target}}$, for example $0, 0.2, \ldots, 1$,
   - κ_0, for example 0 dB, 3 dB, …, 21 dB,
   - κ_{I}, for example 0 dB, 3 dB, …, 21 dB.
2) For all combinations of $\tilde{J}_{\text{target}}$, κ_0 and κ_{I}:
   a) Calculate correlation matrices according to (29), (31), and (32).
   b) Generate multiple realizations of channel matrices according to (33) and (34).
   c) Test the algorithm using the generated channel matrices

VII. Conclusions

We presented an analytical multi-user MIMO channel model that is able to model interference in the spatial domain. The proposed model characterizes the amount of eigenspace alignment on a continuous scale between fully aligned and maximally non-aligned.

The parameterization of the model is exemplified using channel measurements in two different scenarios: peer-to-peer channels in an indoor office environment, and an indoor-to-outdoor cubicle-style office environment. We provided an implementation recipe for ready model use.

It turns out that system performance metrics under interference strongly depends on the alignment of the eigenspaces of the channel matrices of the intended signal and of the interfering channel. For strongly correlated channels, the difference in data rate can reach up to 65 % in a 4×4 MIMO system.

VIII. Acknowledgment

The authors would like to thank Prof. George Papanicolaou, Stanford University, for enlightening discussions on curves in the unitary group.

Appendix

A. Proof of Theorem 1

Following (7), the extreme values of $J(\mathbf{R}_0, \mathbf{V}\mathbf{\Gamma}\mathbf{V}^{\text{H}})$ are found via the optimization over $\mathbf{Q}$

$$\begin{array}{ll} \text{min./max.} & \det\left(\mathbf{I} + \mathbf{\Lambda}\mathbf{Q}(\mathbf{I}+\mathbf{\Gamma})^{-1}\mathbf{Q}^{\text{H}}\right) \\ \text{subject to} & \mathbf{Q}^{\text{H}}\mathbf{Q} = \mathbf{I}, \end{array} \tag{35}$$

where we have absorbed the factor σ^2 into the diagonal matrices as $\mathbf{\Lambda} \leftarrow \mathbf{\Lambda}/\sigma^2$ and $\mathbf{\Gamma} \leftarrow \mathbf{\Gamma}/\sigma^2$.

First, assume that $\mathbf{\Lambda}$ is invertible, i.e., $\lambda_n > 0$. With $\mathbf{\Gamma}' = (\mathbf{I}+\mathbf{\Gamma})^{-1}$, the objective function of (35) can be rewritten as

$$\det\left(\mathbf{I} + \mathbf{\Lambda}\mathbf{Q}(\mathbf{I}+\mathbf{\Gamma})^{-1}\mathbf{Q}^{\text{H}}\right) \tag{36}$$

$$= \det(\mathbf{\Lambda})\det(\mathbf{\Lambda}^{-1} + \mathbf{Q}\mathbf{\Gamma}'\mathbf{Q}^{\text{H}}). \tag{37}$$

The matrices $\mathbf{\Lambda}^{-1}$ and $\mathbf{Q}\mathbf{\Gamma}'\mathbf{Q}^{\text{H}}$ are Hermitian and positive definite with sorted eigenvalues $(\lambda_n^{-1}, \ldots, \lambda_1^{-1})$ and $\left((1+\gamma_n)^{-1}, \ldots, (1+\gamma_1)^{-1}\right)$, respectively. A theorem by Fiedler [21, equation (2)] implies, for all unitary $\mathbf{Q}$,

$$\prod_{i=1}^{n}\left(\lambda_i^{-1} + (1+\gamma_i)^{-1}\right) \tag{38}$$

$$\leq \det(\mathbf{\Lambda}^{-1} + \mathbf{Q}\mathbf{\Gamma}'\mathbf{Q}^{\text{H}}) \tag{39}$$

$$\leq \prod_{i=1}^{n}\left(\lambda_i^{-1} + (1+\gamma_{n+1-i})^{-1}\right), \tag{40}$$

and thus,

$$\begin{aligned} &\prod_{i=1}^{n}\left(1 + \tfrac{\lambda_i}{1+\gamma_i}\right) \\ &\leq \det\left(\mathbf{I} + \mathbf{\Lambda}\mathbf{Q}(\mathbf{I}+\mathbf{\Gamma})^{-1}\mathbf{Q}^{\text{H}}\right) \\ &\leq \prod_{i=1}^{n}\left(1 + \tfrac{\lambda_i}{1+\gamma_{n+1-i}}\right). \end{aligned} \tag{41}$$

The lower and upper bounds are achieved by $\mathbf{Q} = \mathbf{I}$ and $\mathbf{Q} = \overleftarrow{\mathbf{I}}$, respectively.

For the case that $\mathbf{\Lambda}$ is not invertible, we consider the sequence $\{\mathbf{\Lambda}_k; k = 1, 2, \ldots\}$ of invertible matrices $\mathbf{\Lambda}_k = \mathbf{\Lambda} + \mathbf{I}/k$. The diagonal elements of each $\mathbf{\Lambda}_k$ is sorted in descending order. Therefore, (41) holds for each $\mathbf{\Lambda}_k$. Noting that the determinant as well as the left and right hand sides of (41) are continuous in $\mathbf{\Lambda}_k$ (with no singularities), we conclude that the bound must continue to hold for the limit $\lim_{k\to\infty}\mathbf{\Lambda}_k = \mathbf{\Lambda}$.

B. Proof of Theorem 2

First consider the denominator of (11). Equations (9) and (10) imply that

$$J_{\max}(\mathbf{R}_0, \mathbf{\Gamma}) - J_{\min}(\mathbf{R}_0, \mathbf{\Gamma}) = \log_2 \prod_{d=1}^{D} \frac{\sigma^2 + \lambda_{D+1-d} + \gamma_i}{\sigma^2 + \lambda_d + \gamma_i}. \tag{42}$$

This expression remains invariant when $\mathbf{R}_0$ and $\mathbf{R}_{\text{I}}$ (i.e., $\{\lambda_i\}$ and $\{\gamma_i\}$) are exchanged.

Now consider the numerator of (11). Recall equation (7),

$$J(\mathbf{R}_0, \mathbf{R}_{\text{I}}) = \log_2 \det\left(\mathbf{I} + \mathbf{\Lambda}\mathbf{Q}(\sigma^2\mathbf{I} + \mathbf{\Gamma})^{-1}\mathbf{Q}^{\text{H}}\right). \tag{43}$$

It is easy to see that

$$\det(\mathbf{I} + \mathbf{B}\mathbf{C}) = \frac{\det(\mathbf{B} + \mathbf{C}^{-1})}{\det(\mathbf{C}^{-1})}$$

for an arbitrary matrix $\mathbf{B}$ and an invertible matrix $\mathbf{C}$. We apply this fact with $\mathbf{B} = \mathbf{\Lambda}$ and $\mathbf{C} = \mathbf{Q}(\sigma^2\mathbf{I} + \mathbf{\Gamma})^{-1}\mathbf{Q}^{\text{H}}$ to obtain

$$J(\mathbf{R}_0, \mathbf{R}_{\text{I}}) = \log_2 \frac{\det\left(\mathbf{\Lambda} + \mathbf{Q}(\sigma^2\mathbf{I} + \mathbf{\Gamma})\mathbf{Q}^{\text{H}}\right)}{\det(\sigma^2\mathbf{I} + \mathbf{\Gamma})} \tag{44}$$

$$= \log_2 \frac{\det\left(\sigma^2\mathbf{I} + \mathbf{U}\mathbf{\Lambda}\mathbf{U}^{\text{H}} + \mathbf{V}\mathbf{\Gamma}\mathbf{V}^{\text{H}}\right)}{\det(\sigma^2\mathbf{I} + \mathbf{\Gamma})}, \tag{45}$$

where we have used the definition $\mathbf{Q} = \mathbf{U}^{\text{H}}\mathbf{V}$. Setting $\mathbf{U} = \mathbf{V}$ yields an expression for $J_{\min}(\mathbf{R}_0, \mathbf{\Gamma})$, and thus

$$J(\mathbf{R}_0, \mathbf{R}_{\text{I}}) - J_{\min}(\mathbf{R}_0, \mathbf{\Gamma}) \tag{46}$$

$$= \log_2 \frac{\det\left(\sigma^2\mathbf{I} + \mathbf{U}\mathbf{\Lambda}\mathbf{U}^{\text{H}} + \mathbf{V}\mathbf{\Gamma}\mathbf{V}^{\text{H}}\right)}{\det\left(\sigma^2\mathbf{I} + \mathbf{\Lambda} + \mathbf{\Gamma}\right)}. \tag{47}$$

This implies that the numerator of (11) is also invariant under the exchange $\mathbf{R}_0 \leftrightarrow \mathbf{R}_\mathrm{I}$, i.e., $(\mathbf{\Lambda}, \mathbf{U}) \leftrightarrow (\mathbf{\Gamma}, \mathbf{V})$. The proof is complete.

C. Proof of Theorem 3

Recalling (18), minimizing or maximizing $d(\mathbf{R}_0, \mathbf{V}\mathbf{\Gamma}\mathbf{V}^\mathrm{H})$ can be equivalently written as an optimization over $\mathbf{Q}$ as

$$\begin{array}{ll} \text{max./min.} & \mathrm{tr}(\mathbf{\Lambda}\mathbf{Q}\mathbf{\Gamma}\mathbf{Q}^\mathrm{H}) \\ \text{subject to} & \mathbf{Q}^\mathrm{H}\mathbf{Q} = \mathbf{I}. \end{array} \tag{48}$$

We will first prove that the optimum in (48) is achieved by a permutation matrix. In a second step, we show that the particular permutation matrices $\mathbf{I}$ and $\overleftarrow{\mathbf{I}}$ realize the maximum and minimum, respectively.

Since $\mathbf{\Lambda}$ and $\mathbf{\Gamma}$ are diagonal, they can be expressed as $\mathbf{\Lambda} = \sum_{i=1}^n \lambda_i \mathbf{e}_i \mathbf{e}_i^\mathrm{H}$ and $\mathbf{\Gamma} = \sum_{i=1}^n \gamma_i \mathbf{e}_i \mathbf{e}_i^\mathrm{H}$, where $\mathbf{e}_i$ denotes the ith canonical unit vector. Optimization (48) can then be rewritten in terms of the components of $\mathbf{Q} = (Q_{ij})$ as

$$\begin{array}{ll} \text{max./min.} & \sum_{i=1}^n \sum_{j=1}^n \lambda_i \gamma_j |Q_{ij}|^2 \\ \text{subject to} & \sum_i |Q_{ij}|^2 = 1, \quad \forall j \\ & \sum_j |Q_{ij}|^2 = 1, \quad \forall i \\ & \sum_j Q_{ij} Q_{kj}^* = 0, \quad \forall i \neq k. \end{array} \tag{49}$$

Defining new variables $W_{ij} = |Q_{ij}|^2$, for $i, j \in \{1, \ldots, n\}$, and relaxing the last constraint, we arrive at

$$\begin{array}{ll} \text{max./min.} & \sum_{i=1}^n \sum_{j=1}^n \lambda_i \gamma_j W_{ij} \\ \text{subject to} & W_{ij} \geq 0, \quad \forall i, j \\ & \sum_j W_{ij} = 1, \quad \forall i \\ & \sum_i W_{ij} = 1, \quad \forall j. \end{array} \tag{50}$$

Optimization (50) is a linear program with variables W_{ij}. The feasible set is the polytope of doubly stochastic matrices (W_{ij}). By the Birkhoff–von-Neumann theorem [22], the extreme points of the feasible set are permutation matrices, one of which, say $\mathbf{W}_0$, must achieve the optimum. Solution $\mathbf{W}_0$ can be easily mapped back to optimization (48) by setting $\mathbf{Q}_0 = \mathbf{W}_0$, since it consists of elements from $\{0, 1\}$. Moreover, $\mathbf{Q}_0$ is feasible in (48), because permutation matrices are unitary. We have thus shown that there must be a permutation matrix that optimizes (48).

It remains to find the optimal $\mathbf{Q}_0$ among all permutation matrices. To this end, it is natural to represent permutation matrices by invertible functions $\pi : \{1, \ldots, n\} \to \{1, \ldots, n\}$. The objective of (49), as a function of π, is then given as $g(\pi) = \sum_{i=1}^n \lambda_i \gamma_{\pi(i)}$. To study how $g(\cdot)$ varies, consider two permutations φ and ψ. Fix two indices p and q, with $p < q$. Let $\varphi(p) = \psi(q)$, $\varphi(q) = \psi(p)$ and $\varphi(i) = \psi(i)$ for all $i \in \{1, \ldots, n\} \setminus \{p, q\}$, i.e., φ and ψ differ only by a transposition between indices p and q. Without loss of generality, let $\varphi(p) < \varphi(q)$. It follows that

$$g(\varphi) = \sum_{i=1}^n \lambda_i \gamma_{\varphi(i)} \tag{51}$$

$$= \sum_{i=1}^n \lambda_i \gamma_{\psi(i)} + (\lambda_p - \lambda_q)(\gamma_{\varphi(p)} - \gamma_{\varphi(q)}) \tag{52}$$

$$\geq g(\psi). \tag{53}$$

Hence, transpositions $\varphi \xrightarrow{(p,q)} \psi$ with $p < q$ and $\varphi(p) < \varphi(q)$ decrease the value of g. Finally, define the particular permutations $\varphi^\star(i) = i$ and $\psi^\star(i) = n + 1 - i$. For any permutation π, a sequence of g-decreasing transpositions can be constructed that transforms $\varphi^\star$ to $\psi^\star$ and traverses through π. Therefore,

$$g(\varphi^\star) \geq g(\pi) \geq g(\psi^\star), \qquad \text{for all } \pi. \tag{54}$$

The extreme points $\varphi^\star$ and $\psi^\star$ correspond to $\mathbf{Q}_0 = \mathbf{I}$ and $\mathbf{Q}_0 = \overleftarrow{\mathbf{I}}$, respectively. Finally, note that the roles of minimum and maximum are reversed between this argument and Theorem 3, since (18) contains the objective of (48) with a negative sign.

REFERENCES

[1] D.-S. Shiu, G. Foschini, M. Gans, and J. Kahn, "Fading correlation and its effect on the capacity of multielement antenna systems," *IEEE Transactions on Communications*, vol. 48, no. 3, pp. 502–513, March 2000.

[2] R. Blum, "MIMO capacity with interference," *IEEE Journal on Selected Areas in Communications*, vol. 21, no. 5, pp. 793–801, 2003.

[3] S. Shamai and A. Wyner, "Information-theoretic considerations for symmetric, cellular, multiple-access fading channels. i," *IEEE Transactions on Information Theory*, vol. 43, no. 6, pp. 1877–1894, Nov. 1997.

[4] ——, "Information-theoretic considerations for symmetric, cellular, multiple-access fading channels. ii," *Information Theory, IEEE Transactions on*, vol. 43, no. 6, pp. 1895 –1911, Nov. 1997.

[5] D. Tse and S. Hanly, "Multi-access fading channels: Part I: Polymatroid structure, optimal resource allocation and throughput capacities," *IEEE Transactions on Information Theory*, vol. 4, no. 7, pp. 2796–2815, 1998.

[6] S. Hanly and D. Tse, "Multi-access fading channels: Part II: Delay-limited capacities," *IEEE Transactions on Information Theory*, vol. 44, no. 7, pp. 2816–2831, 1998.

[7] H. Dai, A. F. Molisch, and V. H. Poor, "Downlink capacity of interference-limited MIMO systems with joint detection," *Wireless Communications, IEEE Transactions on*, vol. 3, no. 2, pp. 442–453, 2004.

[8] J.-S. Jiang, M. Demirkol, and M. Ingram, "Measured capacities at 5.8 GHz of indoor MIMO systems with MIMO interference," in *Vehicular Technology Conference, 2003. VTC 2003-Fall. 2003 IEEE 58th*, vol. 1, 2003, pp. 388–393 Vol.1.

[9] Y. Liu, T. Wong, and W. Hager, "Training signal design for estimation of correlated MIMO channels with colored interference," *Signal Processing, IEEE Transactions on*, vol. 55, no. 4, pp. 1486–1497, 2007.

[10] X. Chen, Y. Gong, and Y. Gong, "Suppression of directional interference for STBC MIMO system based on beam-forming," in *Communications, Circuits and Systems Proceedings, 2006 International Conference on*, vol. 2, 2006, pp. 983–987.

[11] M. Rahman, E. de Carvalho, and R. Prasad, "Mitigation of MIMO co-channel interference using robust interference cancellation receiver," in *Vehicular Technology Conference (VTC Fall 2007)*, Baltimore, MD, USA, October 2007.

[12] T. Fugen, J. Maurer, C. Kuhnert, and W. Wiesbeck, "A modelling approach for multiuser MIMO systems including spatially-colored interference [cellular example]," in *IEEE Global Telecommunications Conference, 2004. GLOBECOM '04.*, vol. 2, 2004, pp. 938–942 Vol.2.

[13] J. Poutanen, F. Tufvesson, K. Haneda, V.-M. Kolmonen, and P. Vainikainen, "Multi-link MIMO channel modeling using geometry-based approach," *IEEE Trans. Ant. Prop.*, 2011, in press.

[14] N. Czink, B. Bandemer, C. Oestges, T. Zemen, and A. Paulraj, "Subspace modeling of multi-user MIMO channels," in *IEEE VTC Fall 2011*, San Francisco, USA, Sep. 2011.

[15] M. Herdin, N. Czink, H. Ozcelik, and E. Bonek, "Correlation matrix distance, a meaningful measure for evaluation of non-stationary MIMO channels," in *IEEE VTC Spring 2005*, vol. 1, 2005, pp. 136–140 Vol. 1.

[16] R. W. Hamming, *Numerical Methods for Scientists and Engineers*. Dover Publications, 1987.

[17] C. Martin and B. Ottersten, "Asymptotic eigenvalue distributions and capacity for MIMO channels under correlated fading," *IEEE Trans. Wireless Commun.*, vol. 3, no. 4, pp. 1350–1359, July 2004.

[18] C. Oestges, P. Castiglione, and N. Czink, "Empirical modeling of nomadic peer-to-peer networks in office environment," in *IEEE VTC Spring 2011*, Budapest, Hungary, April 2011.

[19] N. Czink, B. Bandemer, G. Vazquez-Vilar, L. Jalloul, C. Oestges, and A. Paulraj, "Spatial separation of multi-user mimo channels," in *IEEE PIMRC 2009*, Tokyo, Japan, September 2009.
[20] C. Oestges and N. Czink, "Empirical investigation of multi-link separation for indoor MIMO channels," in *IEEE PIMRC 2011*, Toronto, ON, September 2011, accepted for publication.
[21] M. Fiedler, "Bounds for the determinant of the sum of hermitian matrices," *Proc. of Amer. Math. Soc.*, vol. 30, no. 1, pp. 27–31, Sep. 1971.
[22] G. M. Ziegler, *Lectures on Polytopes*, ser. Graduate texts in mathematics; 152. New York: Springer-Verlag, 2007.

Nicolai Czink (S'04, M'08) received his Dipl.-Ing. (M.S.) degree in 2004 and Dr.techn. (Ph.D.) degree in 2007, both from Vienna University of Technology, Austria, with distinction. His Ph.D. thesis received an award from the Austrian Electrotechnical Association (OVE). After his Ph.D., he joined Stanford University as a Postdoctoral Researcher on an Erwin Schrdinger Fellowship of the FWF Austrian Science Fund. After that, he became Senior Researcher at the FTW Telecommunications Research Center Vienna, Austria, working on channel modeling, cooperative communications, and intelligent transportation systems.

Bernd Bandemer (S'06) received his Dipl.-Ing. (MS) degree in Electrical and Computer Engineering in 2006 from Ilmenau University of Technology, Ilmenau, Germany. In 2003/04, he was awarded a Fulbright scholarship to study at Purdue University, West Lafayette, Indiana. His experience outside academia includes working as a research intern at Intel Corporation (Santa Clara, California), at Nokia Research Center (Helsinki, Finland), and at the German Aerospace Center (Munich, Germany). He is currently pursuing a Ph.D. degree in Electrical Engineering at Stanford University. His research is centered around interference and cooperation in wireless networks, from both the information-theoretic and signal processing viewpoints.

Claude Oestges received the M.Sc. and Ph.D. degrees in Electrical Engineering from the Université catholique de Louvain (UCL), Louvain-la-Neuve, Belgium, respectively in 1996 and 2000. In January 2001, he joined as a post-doctoral scholar the Smart Antennas Research Group (Information Systems Laboratory), Stanford University, CA, USA. From January 2002 to September 2005, he was associated with the Microwave Laboratory UCL as a post-doctoral fellow of the Belgian Fonds de la Recherche Scientifique (FRS-FNRS). Claude Oestges is presently a FRS Research Associate and Assistant Professor with the Electrical Engineering Department, Institute for Information and Communication Technologies, Electronics and Applied Mathematics, UCL. He also currently serves as an Associate Editor for the IEEE Transactions on Antennas and Propagation and the IEEE Transactions on Vehicular Technology.He is the author or co-author of two books and more than 150 journal papers and conference communications, and was the recipient of the 1999-2000 IET Marconi Premium Award and of the 2004 IEEE Vehicular Technology Society Neal Shepherd Award.

Thomas Zemen (S'03, M'05, SM'10) was born in Mödling, Austria. He received the Dipl.-Ing. degree (with distinction) in electrical engineering from Vienna University of Technology in 1998 and the doctoral degree (with distinction) in 2004. From 1998 to 2003 he worked as hardware engineer and project manager for the radio communication devices department at Siemens Austria. Since October 2003 Thomas Zemen has been with FTW Forschungszentrum Telekommunikation Wien, he leads the department "Signal and Information Processing" since 2008. He is the speaker of the national research network for "Signal and Information Processing in Science and Engineering" funded by the Austrian Science Fund (FWF). His research interests include vehicular channel measurements and modelling, time-variant channel estimation, orthogonal frequency division multiplexing (OFDM), iterative multiple-input multiple-output (MIMO) receiver structures, cooperative communication systems and interference management. Dr. Zemen teaches as external lecturer at Vienna University of Technology and serves as editor for the IEEE Transactions on Wireless Communications. He is the author or co-author of three books chapters and more than 80 journal papers and conference communications.

Arogyaswami Paulraj , Professor Emeritus, Stanford University, is the author of over 400 research papers, two text books and a co-inventor in 52 US patents. Paulraj has won over two dozen awards including the IEEE's Alexander Graham Bell Medal, Technical Achievement Award (SP Society), Fellow grade and several best paper awards. He is a fellow of seven scientific academies including the US National Academy of Engineering and the Royal Swedish Academy of Engineering Sciences. In 1999, Paulraj founded Iospan Wireless Inc - which developed MIMO-OFDMA wireless system. Iospan was acquired in by Intel Corporation in 2003. He was In 2004, Paulraj co-founded Beceem Communications Inc and the company was acquired by Broadcom Corp. in 2010.